

## CHARACTERISTICS OF REYNOLDS STRESSES IN A TURBULENT BOUNDARY LAYER

**Roeland de Kat**

Aerodynamics and Flight Mechanics Group  
University of Southampton  
Tizard, Highfield, Southampton, SO17 1BJ, UK  
r.de-kat@soton.ac.uk

**Bharathram Ganapathisubramani**

Aerodynamics and Flight Mechanics Group  
University of Southampton  
Tizard, Highfield, Southampton, SO17 1BJ, UK  
g.bharath@soton.ac.uk

### ABSTRACT

Reynolds shear-stress events play an important role in turbulent boundary layers. To investigate their origin, we look at time resolved particle image velocimetry data in a streamwise wall-normal plane and investigate the interaction between large and small scale velocity fluctuations and their contribution to normal and shear stresses. Streamwise velocity fluctuations are found to be predominately large scale and wall-normal velocity fluctuations smaller scale. Their interaction results in shear-stress, which is mostly present in intermediate scales. By spatial decomposition of temporal spectra, we find that large spatial scales interact at large time-scales and small spatial scales at small time-scales. From conditioned temporal spectra, we find that large streamwise velocity fluctuations modulate the amplitude of small scales, which contribute to the normal and shear stresses. Conditioned wavenumber-frequency spectra of these small scales shows that the time evolution of small spatial scales is proportional to large scale streamwise velocity fluctuations.

### INTRODUCTION

Understanding Reynolds shear-stress events in a turbulent boundary layer is of crucial importance for modelling and controlling turbulent wall-flows. A lot of effort is put into capturing, characterising, and quantifying structures responsible for momentum transport in wall-bounded turbulent flow: e.g. Katul *et al.* (2006) show the relative importance of ejections and sweeps in an atmospheric boundary layer, Adrian (2007) describes the organisation of hairpin vortices in wall turbulence, Dennis & Nickels (2011a,b) show vortex packets and long structures in a turbulent boundary layer, and Luzano-Durán *et al.* (2012) characterises the three-dimensional structure of momentum transport in turbulent channels.

Recently, the interaction between large scale and small scale velocity fluctuations in streamwise direction has been studied (Hutchins & Marusic 2007a, Mathis *et al.* 2011, and Ganapathisubramani *et al.* 2012) experimentally and

amplification and modulations effects were found. Earlier experiments by Guala *et al.* (2006) show that a considerable amount of mean shear-stress is produced at large scales. The evidence of scale interaction in streamwise direction combined with the considerable amount of mean shear-stress created by large scales, raises the question whether interactions between large and small scales are important contributors to the mean shear-stress and how they manifest themselves.

In this study, we evaluate the interaction between large and small scales that contribute to the shear-stress from time-resolved particle image velocimetry (PIV) data in a stream-wise wall-normal plane of a turbulent boundary layer.

### EXPERIMENTS

Time resolved PIV experiments are performed in a stream-wise wall-normal plane in a turbulent boundary layer in the water tunnel at Cambridge University Engineering Department. The flow is tripped with a glass rod at the beginning of the test-section and PIV measurements are performed 4.5 m downstream of this trip. The nominal flow conditions at the measurement location are  $U \approx 0.65$  m/s,  $\delta \approx 0.1$  m,  $U_\tau \approx 0.027$  m/s, and  $Re_\tau \approx 2700$ . Two PIV experiments with different field-of-view (FOV) are performed. Particle image pairs are captured and processed using LaVision software DaVis 7.2. The first experiment has a large field-of-view (FOV) that covers an area of  $37 \times 4.6$  cm (approximately  $4 \delta \times 0.5 \delta$ ) with a digital resolution of 10 pixels/mm and a total of 25,000 images are acquired in 5 separate sets at 500 Hz. The second experiment has a small FOV that covers an area of  $17 \times 4.5$  cm (approximately  $2 \delta \times 0.5 \delta$ ) with a digital resolution of 22 pixels/mm and a total of 50,000 images are acquired in 10 separate sets at  $f_{acq} = 1$  kHz. Both experiments capture 50 s ( $325 \delta/U$ ) of flow. Images are preprocessed using a min-max normalisation. Vectors are calculated using Gaussian weighted correlation windows (WS) that start at 64 by 64 pixel and finish at 16 by 16 pixels with an overlap factor of 50%. This re-

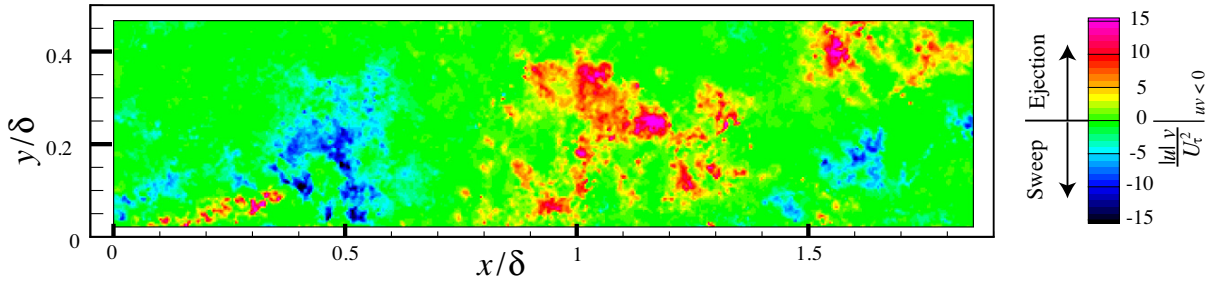


Figure 1. Instantaneous snapshot from the small FOV experiment showing sweeps and ejections.

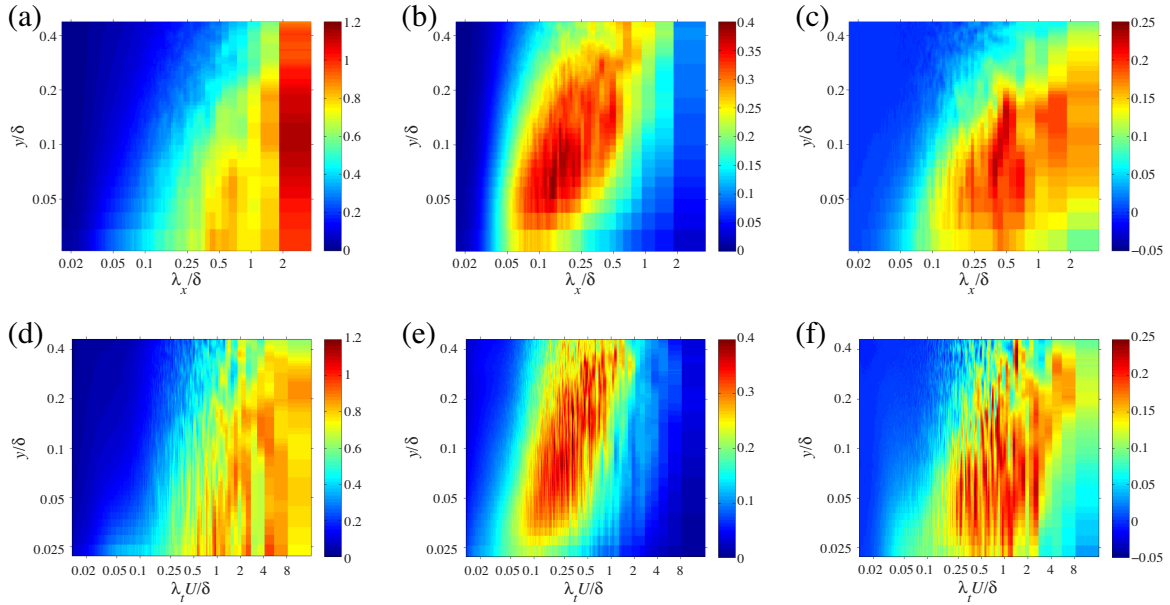


Figure 2. Premultiplied spectra from large FOV measurements (a-c) and small FOV measurement (d-f). The lowest wall-normal locations is  $y/\delta = 0.026$  ( $y^+ = 69$ ) for the large FOV and  $y/\delta = 0.022$  ( $y^+ = 58$ ) for the small FOV. (a) Spatial premultiplied spectrum of streamwise velocity fluctuations,  $\kappa_x \Phi_{uu}^{K_x}/U_\tau^2$ . (b) Spatial premultiplied spectrum of wall-normal velocity fluctuations,  $\kappa_x \Phi_{vv}^{K_x}/U_\tau^2$ . (c) Spatial premultiplied cospectrum of streamwise with wall-normal velocity fluctuations,  $\kappa_x \Phi_{uv}^{K_x}/U_\tau^2$ . (d) Temporal premultiplied spectrum of streamwise velocity fluctuations,  $f \Phi_{uu}^f/U_\tau^2$ . (e) Temporal premultiplied spectrum of wall-normal velocity fluctuations,  $f \Phi_{vv}^f/U_\tau^2$ . (f) Temporal premultiplied cospectrum of streamwise with wall-normal velocity fluctuations,  $f \Phi_{uv}^f/U_\tau^2$ .

sults in a spatial resolution of  $\Delta x^+ = 22$  ( $l^+ = 43$ , WS = 1.6 mm) with a temporal resolution of  $\Delta t^+ = 1.5$  for the large FOV and a spatial resolution of  $\Delta x^+ = 10$  ( $l^+ = 20$ , WS = 0.7 mm) with a temporal resolution of  $\Delta t^+ = 0.7$  for the small FOV. The first valid vector for the large FOV is at  $y/\delta = 0.026$  ( $y^+ = 69$ ) for the small FOV at  $y/\delta = 0.022$  ( $y^+ = 58$ ).

## RESULTS

We want to gain insights into momentum transport or shear-stress, which is the interaction between streamwise,  $u$ , and wall-normal,  $v$ , fluctuations. The shear-stress in wall bounded turbulence is primarily caused by sweeps and ejections. The range of scales within sweeps and ejections increases with increasing Reynolds number. An example of an instantaneous field of sweeps and ejections (figure 1) shows that, for the current (moderate) Reynolds number, large regions of sweep and ejection already exist, which contain numerous smaller structures within them. Quantifying the range of space and time-scales and the inter-

actions between them will help to understand momentum transport in turbulent boundary layers and potentially lead to new ideas on how to manipulate them.

We first look into the energy contents in space and time of normal and shear stresses for different wall-normal locations (figure 2). Spatial premultiplied power spectra are determined from the large FOV. The full length of the FOV is used and after applying a Hamming window the spectra are determined. The spectra are averages over 25,000 blocks. The spatial energy distribution  $\kappa_x \Phi_{uu}^{K_x}$  of  $u$  over different wavelengths,  $\lambda_x$  (with  $\kappa_x = 1/\lambda_x$ ), figure 2(a), shows that, even though the spectrum of the streamwise velocity fluctuations is truncated—due to limited streamwise extent of the domain—, most of the energy in streamwise direction is present in scales larger than  $\delta$ . This is in line with the results of Hutchins & Marusic (2007b), who find that, except for the viscous inner region, most of the energy is present in larger scales. The spatial energy distribution for wall-normal velocity fluctuations  $\kappa_x \Phi_{vv}^{K_x}$ , figure 2(b), shows that most energy is present in scales smaller than  $\delta$ . The peak in the cospectrum  $\kappa_x \Phi_{uv}^{K_x}$ , lies in between the peak contribu-

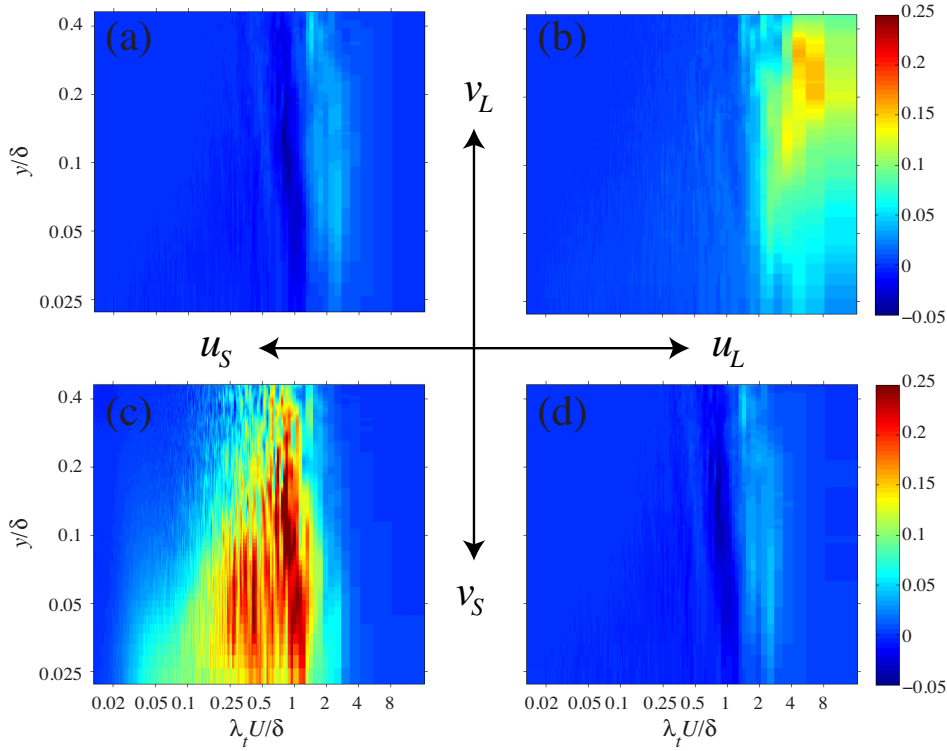


Figure 3. Decomposition of temporal premultiplied cospectrum. The lowest wall-normal locations is  $y/\delta = 0.022$  ( $y^+ = 58$ ). (a) Small scale streamwise velocity fluctuations,  $u_S$ , with large scale wall-normal velocity fluctuations,  $v_L$ ,  $f\Phi_{u_S v_L}^f/U_\tau^2$ . (b) Large scale streamwise velocity fluctuations,  $u_L$ , with large scale wall-normal velocity fluctuations,  $v_L$ ,  $f\Phi_{u_L v_L}^f/U_\tau^2$ . (c) Small scale streamwise velocity fluctuations,  $u_S$ , with small scale wall-normal velocity fluctuations,  $v_S$ ,  $f\Phi_{u_S v_S}^f/U_\tau^2$ . (d) Large scale streamwise velocity fluctuations,  $u_L$ , with small scale wall-normal velocity fluctuations,  $v_S$ ,  $f\Phi_{u_L v_S}^f/U_\tau^2$ .

tions in the streamwise and wall-normal fluctuations (figure 2(c)). This shows that the peak in contribution to the mean Reynolds shear-stress,  $\overline{uv}$ , is between  $0.25 \delta$  and  $2 \delta$ .

Time-scales of the stresses are assessed by temporal premultiplied power spectra, which are determined from the small-FOV, and are shown in figure 2(d-f). The time series from the small FOV are divided into blocks of 2.5 s ( $16 \delta/U$ ) with 50% overlap and after applying a Hamming window the spectra are determined. To minimise potential effects of aliasing, the spectra are filtered with a Gaussian filter, which has a cut-off frequency of  $f_{acq}/3$ . Spectra are averaged per wall-normal location over all blocks and all points in streamwise direction. The resulting spectra are averages over 15,000 blocks. The temporal energy distribution  $f\Phi_{uu}^f$  of  $u$  over different time-scales  $\lambda_t$  ( $f = 1/\lambda_t$ ) is shown in figure 2(d). It indicates a similar behaviour for the temporal scales as for the spatial scales shown in figure 2(a), however, due to a large time series, energy for a larger range of time-scales can be determined. The temporal energy distribution for wall-normal velocity fluctuations  $f\Phi_{vv}^f$ , figure 2(e), shows that most of the energy is present in time-scales smaller than  $\delta/U$ . The cospectrum  $f\Phi_{uv}^f$ , figure 2(f), shows that the major contribution to the mean Reynolds shear-stress,  $\overline{uv}$ , is from the time-scales between  $0.25 \delta/U$  and  $4 \delta/U$ .

There is a scale separation in time and space between the streamwise and wall-normal velocity fluctuations. The peak contribution to mean shear-stress lies in-between these peaks and raises the question how the different scales interact to contribute to shear. Hutchins & Marusic (2007a),

Mathis *et al.* (2011), and Ganapathisubramani *et al.* (2012) found an amplitude modulation effect of large streamwise velocity scales on small streamwise velocity scales. To see how the interaction between large and small scales contributes to the mean shear-stress, we decompose velocity signals into large and small scales based on the separation in energy containing temporal and/or spatial scales in streamwise and wall-normal velocity fluctuations.

### Link between space and time

To evaluate whether a direct relation between large and small scale structures that contribute to the mean shear-stress exists, we decompose the spatial signal into large and small spatial scales by filtering the spatial signal with a top-hat filter with length  $\delta$  to obtain  $u_L$  and  $u_S$ , and  $v_L$  and  $v_S$ . The resulting shear-stress contributions then become:

$$uv = u_L v_L + u_L v_S + u_S v_L + u_S v_S \quad (1)$$

Subsequently, temporal premultiplied cospectra are determined for the different combinations of large and small scale spatial structures (following the same procedure as before) and are shown in figure 3. The interaction between  $u_S$  and  $v_L$ ,  $f\Phi_{u_S v_L}^f$ , figure 3(a), shows that this combination of scales contributes little to the mean shear-stress, which is in line with what one would expect based on their individual energy content. The interaction between  $u_L$  and  $v_L$ ,  $f\Phi_{u_L v_L}^f$ , figure 3(b), shows that this combination of scales

contributes to the mean shear-stress further from the wall, indicating that, further from the wall, large scale structures (both in space and time) are an important contributor to the mean shear-stress. The interaction between  $u_S$  and  $v_S$ ,  $f\Phi_{u_S v_S}^f$ , figure 3(c), shows that this combination of scales contributes to the mean shear-stress closer to the wall, indicating that, close to the wall, small scale structures (both in space and time) are an important contributor to the mean shear-stress. The interaction between  $u_L$  and  $v_S$ ,  $f\Phi_{u_L v_S}^f$ , figure 3(d), shows that this combination of scales only has a small contribution to the mean shear-stress. This is in contrast with their individual energy content, from which one could expect that the most energetic spatial scales of  $u$  and  $v$  will interact to contribute to the mean shear-stress in intermediate time-scales.

The absence of strong cross terms (figure 3(a and d)) shows that large spatial scales only interact at large time-scales and small spatial scales only interact at small time-scales. This suggests that large scales (in space and time) and small scales only directly interact with themselves and not with each other. Even though no direct link seems to exist between different temporal and spatial scales, the influence of large scales on small scales could manifest itself as amplitude modulation, such as found for streamwise velocity fluctuations (Hutchins & Marusic, 2007a, Mathis *et al.*, 2011, and Ganapathisubramani *et al.*, 2012).

### Amplitude modulation of small-scales

To assess the effect of the large scale on the amplitude of small scales, we decompose the temporal signal into large and small time-scales and look at conditioned temporal spectra of small scales. The reader should note that, except for wall-normal location, we are not using spatial information for this part of the analysis. Large time-scales  $U_{LT}$  are determined by filtering each run with a Hanning filter of  $2\delta/U$  in time, which has a full width at half max of  $\delta/U$ . Small-scale fluctuations are the difference between the original velocity signal and this large-scale signal. The resulting small scale signal is divided into  $2\delta/U$  blocks that have an overlap of 50%. Large scales fluctuations are divided into four bins based on the value of  $U_{LT}$  at the centre of each block, each containing roughly 25% of the occurrences and, therefore, we will refer to it as quartiles. The lower quartile contains all values of  $U_{LT} < \bar{U}_{LT} - 0.75\sigma_{U_{LT}}$ , the inner lower quartile contains all values of  $\bar{U}_{LT} - 0.75\sigma_{U_{LT}} < U_{LT} < \bar{U}_{LT}$ , the inner upper quartile contains all values of  $\bar{U}_{LT} < U_{LT} < \bar{U}_{LT} + 0.75\sigma_{U_{LT}}$ , upper quartile contains all values of  $U_{LT} > \bar{U}_{LT} + 0.75\sigma_{U_{LT}}$  (see insets in figure 4). For each bin, the spectral content of the small scale is determined by windowing each block by a Hanning filter and averaging the spectra. Spectra are averaged per wall-normal location over all blocks in each bin and over all points in streamwise direction. The resulting conditioned spectra are averages of circa 40,000 blocks per bin. To minimise potential effects of aliasing, the spectra are filtered with a Gaussian filter, which has a cut-off frequency of  $f_{acq}/3$ . The average of the conditioned spectra results in the unconditioned spectra for the small scales.

The conditioned streamwise, wall-normal, and shear-stress energy content are shown in figure 4. The energy content of the small scale streamwise velocity fluctuations (figure 4 (a, d, g, j)) shows that close to the wall ( $y/\delta < 0.1$ ), the amplitude of small scale fluctuations is increasing with increasing large scale velocity. Farther away from the wall ( $y/\delta > 0.1$ ), an opposite trend can be observed and the

amplitude of small scale fluctuations is decreasing with increasing large scale velocity. A similar trend in amplitude modulations was observed by Ganapathisubramani *et al.* (2012).

The energy content of the wall-normal fluctuations (figure 4(b, e, h, k)) shows a similar trend to the streamwise fluctuations in the near wall region and far away from the wall. However, in the region  $0.05 < y/\delta < 0.15$  peak values appear in the inner quartiles. This suggests that additional influences (such as phase differences) on the energetic small scales in wall-normal velocity fluctuations exist.

The contribution to the mean shear-stress figure 4(c, f, i, l) shows that for  $y/\delta < 0.1$  more shear-stress contribution is present for  $U_{LT} > \bar{U}_{LT}$  and less shear-stress contribution is present for  $U_{LT} < \bar{U}_{LT}$ . For  $y/\delta < 0.1$  this trend is reversed and more shear-stress contribution is present for  $U_{LT} < \bar{U}_{LT}$  and less shear-stress contribution is present for  $U_{LT} > \bar{U}_{LT}$ . For the region  $0.025 < y/\delta < 0.1$ , the peak shear-stress contribution is in the inner upper quartile, this suggests that, similar to the wall-normal fluctuations, additional influences play a role for shear-stress contribution.

All these conditioned spectra show that the amplitude of small scale velocity fluctuations and contributions to mean shear-stress are significantly influenced by large (time) scale streamwise velocity fluctuations. Further investigations are needed to explore this relation. This could result in a predictive relation—similar to the model proposed by Mathis *et al.* (2011) for inner-outer interaction of streamwise velocity—between large (outer) time-scales of streamwise velocity and small time-scales of normal and shear-stresses.

These results indicate that large time-scale streamwise velocity fluctuations interact/influence small scale normal and shear stresses in time. To assess what the space-time evolution of these smaller scales are, we need to look at conditioned wavenumber-frequency spectra.

### Space time evolution of small-scales

To see how the small scale fluctuations of the shear-stress contributions evolve in space and time, we apply a block filter in space-time with size  $\delta \times \delta/U$  in space and time, respectively, to represent the large time-space scales  $U_{LTS}$ . Subsequently, conditioned cospectra of small time-space scales,  $u_{STS}$  and  $v_{STS}$ , are determined by windowing the  $\delta \times \delta/U$  with a Hanning function. The spectra are averages over approximately 160 blocks per bin. The resulting cospectrum contains fluctuations for scales that are smaller than  $\delta/2$  and  $\delta/2U$  in space and time, respectively.

Conditioned wavenumber-frequency cospectra for  $y/\delta = 0.1$  (figure 5) show the time-space evolution for different  $U_{LTS}$ . For the lower quartile, figure 5(a), the ridge in cospectral density aligns with  $f = -0.9\kappa_x U$ . For the inner lower quartile, figure 5(b), the ridge in cospectral density appears to align with  $f = -\kappa_x U$ . For the inner upper quartile, figure 5(c), the ridge in cospectral density appears to have a slightly large slope than  $f = -\kappa_x U$ . Lastly, the ridge in cospectral density for the upper quartile, figure 5(d), aligns with  $f = -1.1\kappa_x U$ . Similar results were found for the streamwise and wall-normal fluctuations.

These results indicate that similar waves numbers (spatial energy contents) evolve up to 10% slower in time for lower  $U_{LTS}$  and up to 10% faster in time for higher  $U_{LTS}$ . This could indicate that frequency modulation, such as observed by Ganapathisubramani *et al.* (2012), is caused by similar spatial scales evolving faster or slower in time due

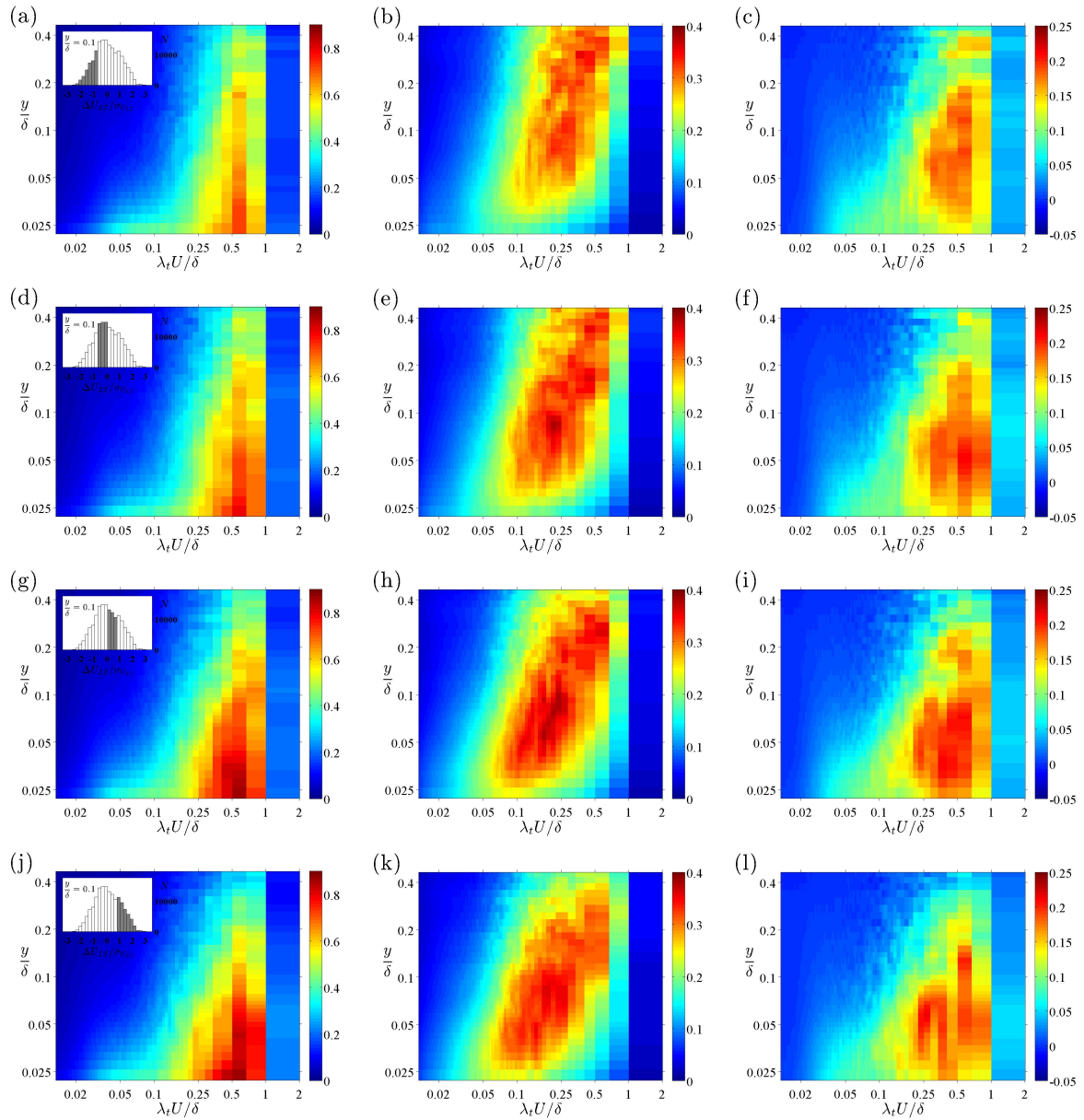


Figure 4. Conditioned premultiplied temporal spectra from small FOV measurements. The lowest wall-normal locations is  $y/\delta = 0.022$  ( $y^+ = 58$ ). Increasing  $U_{LT}$  per row. (a-c) Lower quartile of  $U_{LT}$ . (d-f) Inner lower quartile of  $U_{LT}$ . (g-i) Inner upper quartile of  $U_{LT}$ . (j-k) Upper quartile of  $U_{LT}$ . Insets in (a, d, g, and j) show the histogram of  $U_{LT}$  for  $y/\delta = 0.1$  with the corresponding bin highlighted in grey ( $\Delta U_{LT} = U_{LT} - \bar{U}_{LT}$ ). (a, d, g, and j) Streamwise fluctuations,  $f\Phi_{u_{ST}u_{ST}}^f/U_{\tau}|_{U_{LT}}$  (b, e, h, and k) Wall-normal fluctuations,  $f\Phi_{v_{ST}v_{ST}}^f/U_{\tau}^2|_{U_{LT}}$  (c, f, i, and l) Cospectra,  $f\Phi_{u_{ST}v_{ST}}^f/U_{\tau}^2|_{U_{LT}}$ . (Not all wall-normal locations are shown)

to higher or lower  $U_{LT}$ s.

## SUMMARY

Time-resolved PIV was performed in a turbulent boundary layer for two different FOVs. Space spectra and time spectra show that there is a scale-separation between streamwise and wall-normal fluctuations. Temporal cospectra of a decomposition of the spatial scales in large and small spatial scales, shows that large scales evolve at large time-scales and small scales evolve at small time-scales. Temporal spectra and cospectra conditioned on large time-scales of streamwise velocity fluctuations, show that these large time-scale streamwise fluctuations modulate the

amplitude of small scale fluctuation in normal and shear stresses. Wavenumber-frequency cospectra conditioned on large scale (in time and space) streamwise velocity fluctuations show that for small space-time scales the spatial scales evolve faster in time for higher large scale velocity.

## REFERENCES

- Adrian, R.J. (2007) Hairpin vortex organization in wall turbulence. *Phys. Fluids*, **19**, 041301
- Dennis, D.J.C. and Nickels, T.B. (2011a) Experimental measurement of large-scale three-dimensional structures in a turbulent boundary layer. Part 1. Vortex packets. *J. Fluid Mech.*, **673**:180–217.

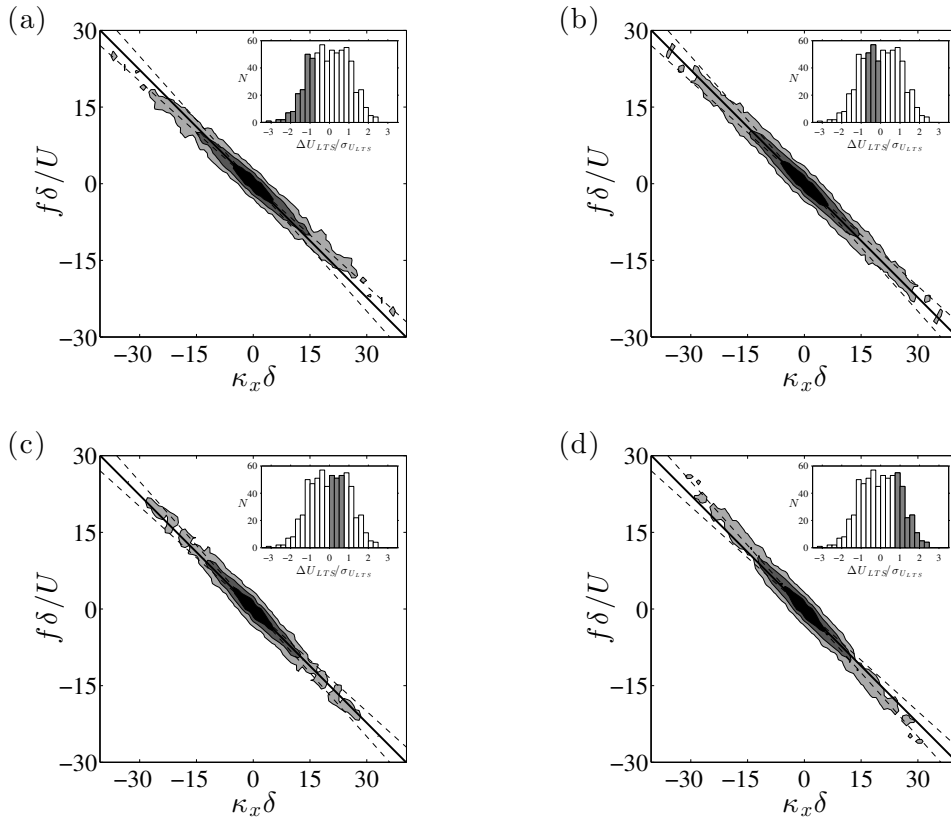


Figure 5. Conditioned cospectra of streamwise with wall-normal small scale velocity in wavenumber-frequency planes for different  $U_{LTS}$  at  $y/\delta = 0.1$ ,  $f\Phi_{u_{STS}v_{STS}}^f/U_{LTS}^2|U_{LTS}$ . Contour levels are in arbitrary units and indicate increases of factor 10. The solid black line indicates  $f = -\kappa_x U$ . Dashed lines indicate  $\pm 10\%$  in slope. Insets show the histogram of  $U_{LTS}$  with the corresponding bin highlighted in grey ( $\Delta U_{LTS} = U_{LTS} - \bar{U}_{LTS}$ ). (a) Lower quartile. (b) Inner lower quartile. (c) Inner upper quartile. (d) Upper quartile.

Dennis, D.J.C. and Nickels, T.B. (2011b) Experimental measurement of large-scale three-dimensional structures in a turbulent boundary layer. Part 2. Long structures. *J. Fluid Mech.*, **673**:218–244.

Ganapathisubramani, B., Hutchins, N., Monty, J.P., Chung, D., and Marusic, I. (2012) Amplitude and frequency modulation in wall turbulence. *J. Fluid Mech.*, doi:10.1017/jfm.2012.398

Guala, M., Hommema, S.E., and Adrian, R.J. (2006) Large-scale and very-large-scale motions in turbulent pipe flow. *J. Fluid Mech.*, **554**:521–542.

Hutchins, N. and Marusic, I. (2007a) Large-scale influences in near-wall turbulence. *Phil. Trans. R. Soc. A*, **365**:647–664.

Hutchins, N. and Marusic, I. (2007b) Evidence of very long meandering features in the logarithmic region of turbulent boundary layers. *J. Fluid Mech.*, **579**:467–477.

Katul, G., Poggi, D., Cava, D., Finnigan, J. (2006) The relative importance of ejections and sweeps to momentum transfer in the atmospheric boundary layer. *Boundary-Layer Meteorol.*, **120**:367–375.

Luzano-Durán, A., Flores, O., and Jiménez, J. (2012) The three-dimensional structure of momentum transfer in turbulent channels. *J. Fluid Mech.*, **694**:100–130.

Mathis, R., Hutchins, N., and Marusic, I. (2011) A predictive inner-outer model for streamwise turbulence statistics in wall-bounded flows. *J. Fluid Mech.*, **681**:537–566.